scientific reports

OPEN

Jet mixing optimization using a bio-inspired evolution of hardware and control

Tamir Shaqarin[2,6], Zhutao Jiang[1,6], Tianyu Wang[1], Chang Hou[1], Guy Y. Cornejo Maceda[1,3✉], Nan Deng[1], Nan Gao[1,4] & Bernd R. Noack[1,5✉]

Jet mixing is a critical factor in various engineering applications, influencing pollutant dispersion, chemical processes, medical treatments, and combustion enhancement. Hitherto, jet mixing has typically been optimized by either passive or active control techniques. In this experimental study, we combine simultaneous optimization of active control with 12 inward-pointing minijets and a tuneable nozzle exit shape commanded by 12 stepper motors. Jet mixing is monitored at the end of the potential core with an array of 7×7 Pitot tubes. This high-dimensional actuation space is conquered with Particle Swarm Optimization through Targeted, Position-Mutated Elitism. Our results underscore the significant impact of combining control techniques, illustrating the complex interactions of both passive and active control on jet flow dynamics. The mixing area of the combined control optimization is 4.5 times larger than the area of the unforced state. This mixing increase significantly outperforms the effect of shape optimization of the nozzle alone. Our study points at the potential of optimization in high-dimensional design spaces for shapes as well as passive and active control—leveraging the rapid development of flow control hardware and the increasingly powerful tools of artificial intelligence for optimization.

Keywords Flow control, Jet mixing, Bio-inspired optimization, Smart nozzle

The study of jet mixing has been a focal point in fluid mechanics. When the fluid is ejected from the nozzle, the shear layer at the nozzle outlet gradually expands on both the inner and outer sides, forming the jet mixing layer. Within this layer, coherent structures or large-scale periodic vortices are generated. Adjacent vortices undergo pairing, causing fluid to be entrained into the mixing layer and increasing its thickness along the jet direction. A key characteristic of the jet flow is its capacity to draw in more fluid from the surrounding environment, facilitated by the mixing layer. Efficient and fast mixing is the key to improving gas burners, chemical reactors, and other devices.

Decades of extensive research in jet mixing control have highlighted the ongoing need for innovative and highly efficient control approaches. Generally, these approaches are classified into passive and active control based on whether energy is injected into the flow field. Passive methods typically involve modifying the nozzle exit shape or integrating fixed devices such as tabs to enhance mixing efficiency. For instance, Quinn's studies[1,2] on non-circular jets, such as triangular or elliptical jets, highlight the importance of azimuthal curvature variation at the jet exit for improving mixing. Ethirajan's research[3] specifically examines how tab length influences jet mixing control. Lin et al.[4] use a lobed mixer to effectively enhance the mixing and combustion of gas and air, increasing the combustion efficiency by 8.318%. Recently, bio-inspired flow control methods have gained prominence, leveraging natural systems to enhance flow performance. These approaches exploit the physiological attributes of living creatures to improve jet flow control. For instance, inspired by shark fins, Gad-el-Hak et al.[5] integrated fins into the nozzle design, resulting in improved jet mixing in a passive manner. This innovation significantly reduced jet impact vibration amplitude by 85% downstream from the rod bundle. Active flow control methods inject energy, enhance the instability at the jet exit, or create new flow structures to manipulate the jet flow

[1]Chair of Artificial Intelligence and Aerodynamics, School of Mechanical Engineering and Automation, Harbin Institute of Technology, Shenzhen 518055, People's Republic of China. [2]Department of Mechanical Engineering, Tafila Technical University, Tafila 66110, Jordan. [3]Department of Aerospace Engineering, Universidad Carlos III de Madrid, Av. de la Universidad, 30, Leganés 28911, Madrid, Spain. [4]Department of Mechanical Engineering, University of New Brunswick, Fredericton E3B 1B5, NB, Canada. [5]Guangdong Provincial Key Laboratory of Intelligent Morphing Mechanisms and Adaptive Robotics, Harbin Institute of Technology, Shenzhen 518055, People's Republic of China. [6]These authors contributed equally: Tamir Shaqarin and Zhutao Jiang. ✉email: yoslan@hit.edu.cn; bernd.noack@hit.edu.cn

dynamics. Samimy et al.[6] employed eight plasma actuators at the jet exit to excite various instabilities. Yang et al.[7] use two minijets as actuators to increase jet mixing. Thanks to the energy injection, the velocity at the end of the original jet core area is reduced by approximately 30%, significantly outperforming passive control schemes such as elliptical ones, which achieve only a few percent reduction[8]. Although both passive and active control methods have significantly advanced jet mixing, combining active and passive control, while optimizing the number of actuators, may achieve more powerful and effective flow control.

Complex flow control devices present a high-dimensional parameter space to explore. Given the huge search space and time constraints, there is a critical need for effective and rapidly converging optimization algorithms. The high number of manipulation variables motivates data-driven control strategies such as online optimization, artificial intelligence (AI), machine learning control (MLC), reinforcement learning (RL)[9], etc. Data-driven control has been used recently for turbulent flows with a multitude of sensors and actuators and has proven its efficiency[10-13]. It has the advantage of exploring the large search space to find the "most capable" flow control strategy. Wu et al.[14] employed a bio-inspired genetic algorithm (GA), simulating the survival of the fittest in biological evolution, to optimize the airfoil shape. Similarly, Koumoutsakos et al.[15] used evolutionary strategies (ES) to optimize parameters such as amplitude, frequency, and phase for slot-jet active control actuators in controlling compressible jets. Xu et al.[16] utilized a particle swarm algorithm, inspired by animal group predation behavior, for in-loop design optimization to enhance synthetic jets for controlling separation on a backward-facing step. These bio-inspired algorithms excel in navigating high-dimensional, complex parameter spaces to achieve optimization goals efficiently.

The concept of this study is depicted in Fig. 1. On the hardware side, we draw inspiration from avian flight mechanics. The flexible wings of birds provide exceptional maneuverability, enabling a range of flight behaviors including emergency stops and gliding. During emergency stops, birds' wings slightly bend forward, and the feathers on the wings spread, blocking the flow of the wing's lower surface and facilitating high angle of attack (AOA) maneuvers. During gliding, eagles spread their wings to both sides of their bodies, and their wingtip feathers curl upwards, reducing induced drag and enhancing flight efficiency. Building on these observations,
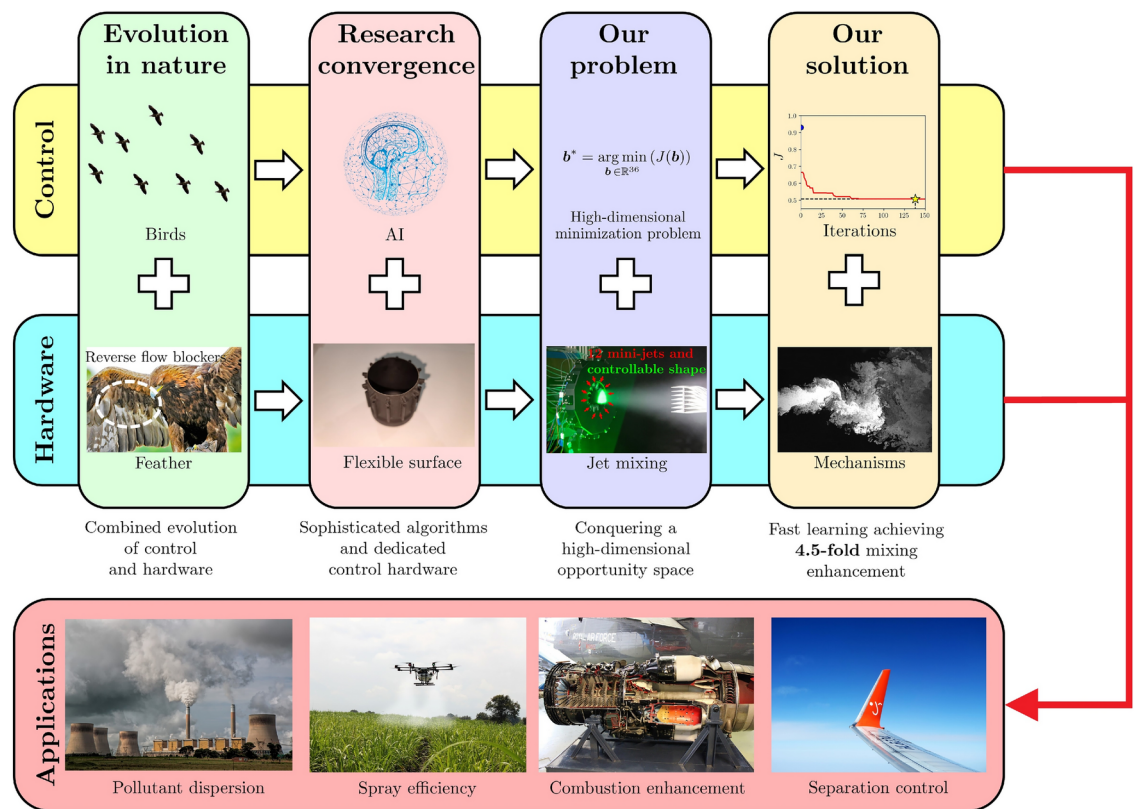
Figure 1. Biologically inspired jet mixing experiment. Natural evolution gives rise to efficient evolutionary strategies and efficient flow control hardware. Inspired by mother nature, a new research convergence emerges by combining sophisticated algorithms and dedicated flow control hardware. In this research, we optimize jet mixing enhancement via shape variation and flow control in a high-dimensional opportunity space and fast learning. In our problem, b^* represents the optimal actuation parameters that minimize the cost function J. With the help of the fast learning algorithm, a 4.5-fold mixing area is achieved. This bio-inspired jet mixing enhancement experiment can be applied to a wide variety of applications ranging from pollutant control to flow control with distributed inputs and distributed outputs (DIDO). Images of flexible surface, jet mixing and mechanisms are provided by Zhutao Jiang. The images of birds, feather, pollutant dispersion, spray efficiency, combustion enhancement, and separation control are downloaded from the website: http://pixabay.com.
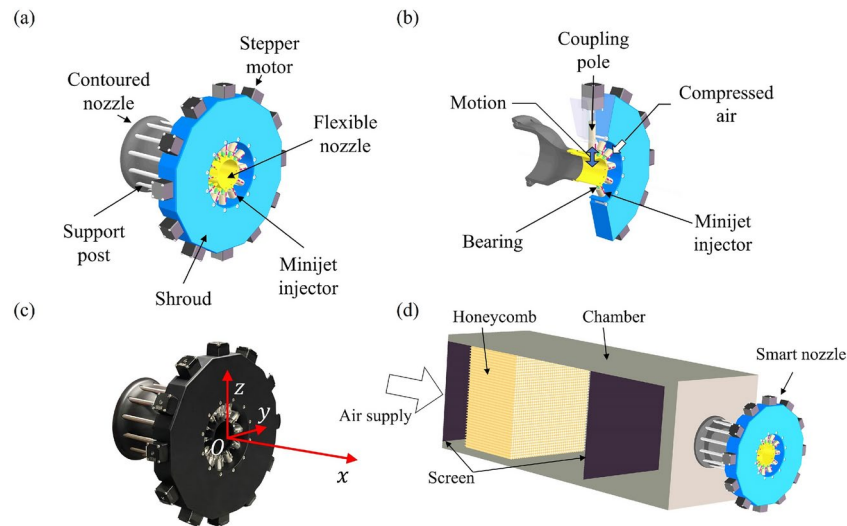
Figure 2. A graphic introduction of the Smart Nozzle, a jet mixing enhancement device featuring simultaneous shape variation and active control. (**a**) the 3D schematic of the Smart Nozzle; (**b**) the section view of the Smart Nozzle highlighting the installation of stepper motors and minijet injectors; (**c**) the physical Smart Nozzle and the Cartesian coordinate system employed in this study; (**d**) the installation of the Smart Nozzle on the chamber to complete the jet mixing facility.

we combine flexible shapes and actuators to achieve improved jet mixing. Over the years, continuous research on rapid prototyping technologies such as 3D printing or the replication molding process has led to significant advancements in processing accuracy, structural complexity, and material diversity. These advances have enabled complex hardware to facilitate flow control concepts derived from natural evolution. In our study, we employed flexible materials (silica gel) to fabricate a jet nozzle and strategically installed minijet actuators, integrating both passive and active control mechanisms. This is the first time passive (shape) and active control methods are integrated for jet mixing control. Combining these methods dramatically expands the control authority over the flow.

However, the simultaneous optimization of shape and active control significantly increases the complexity of the design space. Recently, AI control has been employed for turbulent flows using a multitude of sensors and actuators, demonstrating its efficiency. On the algorithmic side, we employ an innovative particle swarm optimization method named particle swarm optimization through targeted, position-mutated elitism (PSO-TPME)[17]. The well-known particle swarm algorithm (PSO)[18], inspired by the collective intelligence of bird flocks during hunting, serves as the guiding principle for this approach. PSO simulates the hunting behavior of bird flocks, where each bird (particle) continuously adjusts its speed and position based on its own experience and the group's experience to find better solutions. The PSO-TPME algorithm used in this study further incorporates mutations and elitism derived from natural evolution into the well-known PSO algorithm, achieving faster convergence and more accurate learning. With the help of the algorithm's fast optimization capabilities in high-dimensional parameter spaces, we can perform a large number of iterations within a limited time budget to identify efficient control parameters.

This work addresses these challenges through the shape and active optimization of a jet for mixing enhancement. Jet mixing enhancement is one of the main flow control branches crucial to the transportation industry[15,19,20]. The scramjet's efficiency is highly improved with the mixing enhancement through the combustion chamber[21,22]. Enhancing the mixing of the gas plumes of military fighters with cold ambient air reduces their infrared signals and, consequently, their detectability[23]. Jet mixing enhancement is also crucial in chemical reactors and combustion chambers. Jet mixing enhancement inside combustion chambers improves combustion efficiency and reduces emissions[24]. Efficient jet mixing in batch reactors is crucial for monodisperse nanoparticle production since it is vital to coping with fast particle nucleation and growth[25].

We can summarize our main contributions as follows:

1 Bio-inspired hardware and algorithm

    (a) *Experimental setup* To maximize the effectiveness of jet mixing, we constructed the Smart Nozzle, a naturally inspired flexible jet nozzle with peripherally distributed active actuators. The hardware configuration, which provides a benchmark platform for simultaneous shape and control optimization, has a high potential for jet mixing enhancement, whereas it imposes a multitude of actuator parameters and sensors, leading to a broad control design space.

    (b) *PSO-TPME* We implemented a fast-converging and accurate learning algorithm to cope with the high-dimensional jet mixing experiment. Particle swarm optimization through targeted, position-mutated elitism (PSO-TPME) employs several naturally inspired operators on the well-known PSO; classification, targeted mutation, and elitism resulting in early exploration capabilities with fast convergence.

2 Data analysis with machine learning methods

(a) *PDT* We characterize the topology of the flow field with persistent data topology (PDT)[26]. PDT extracts local, global, interior, and one-sided extrema based on a neighborhood analysis and quantifies their topological persistence against noise.

(b) *PIV and clustering* We visualize the flow field under optimum parameters to explore the underlying flow physics via particle image velocimetry (PIV). We employed cluster-based analysis to analyze the characteristics of the actuated flow. The proposed clustering approach automatically extracts flow dynamics from the sampled PIV data.

Results
Methodology
Drawing inspiration from the remarkable ability of natural evolution to produce highly specialized flow control mechanisms, we present a cutting-edge experimental device - the Smart Nozzle - designed to enhance jet mixing efficiency (see Fig 2 for detailed configuration). This innovative hardware features a flexible nozzle shape and a distributed array of active actuators. Specifically, the nozzle shape can be varied using 12 azimuthally deployed stepper motors, while 12 minijet actuators located near the nozzle exit enable the adjustment of frequencies, duty cycles, and phases for active control. To monitor the mixing efficiency under different shape and control parameters, we position an 7×7 array of velocity probes at $6D$ (D represents the jet exit diameter) downstream. Unlike the commonly used centerline velocity[27], we used a total of 49 velocity probes. This configuration provides a low-resolution measurement area, effectively avoiding the problem of the centerline single-point sensor being unable to capture the flow when the controlled jet deviates from the centerline. The Smart Nozzle represents a state-of-the-art benchmark platform for jet mixing efficiency optimization. Leveraging the power of artificial intelligence, we are able to identify the most effective nozzle shape and control parameters for achieving maximum performance.

The optimization problem for jet mixing enhancement is graphically and mathematically formulated in the first row of Fig 3. To achieve optimal performance, we independently control the motions of the 12 azimuthally-deployed stepper motors to vary the nozzle shape, while the 12 minijets are commanded to periodically excite the flow with one frequency and azimuthally-varying duty cycles and phases. This results in a total of 36 optimization parameters which include 12 shapes and 24 active control parameters, respectively. Compared with previous studies[6,7,15], we not only combine passive control with active control but also increase the number
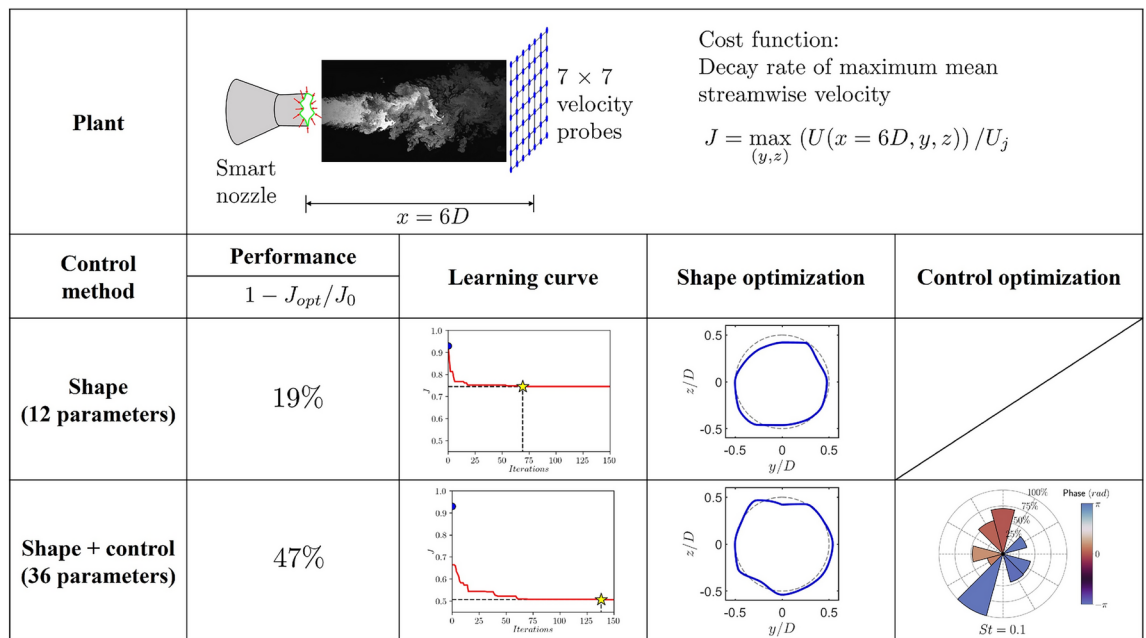

Figure 3. Jet mixing optimization using PSO-TPME. The first row represents the experimental configuration (including shape variation, active control, and downstream sensing) and the calculation of the corresponding cost function J. Here, U represents the mean streamwise velocity measured from the 7×7 velocity probes at $6D$ downstream. For two experimental campaigns (shape and shape + control optimizations), the optimization performance, learning curve, and optimized shape and control parameters are visualized in the figure. The performance column lists the relative cost function reduction $1 - J_{\mathrm{opt}}/J_0$. In the "Learning curve" column, we present the relationship between the number of iterations and the current optimal cost. In the "Shape optimization" column, the optimized nozzle shapes for each case are displayed. In the "Control optimization" column, we show the optimized frequency (non-dimensionalized as the Strouhal number St), with the polar charts representing the optimal duty cycles and phases of active actuators.
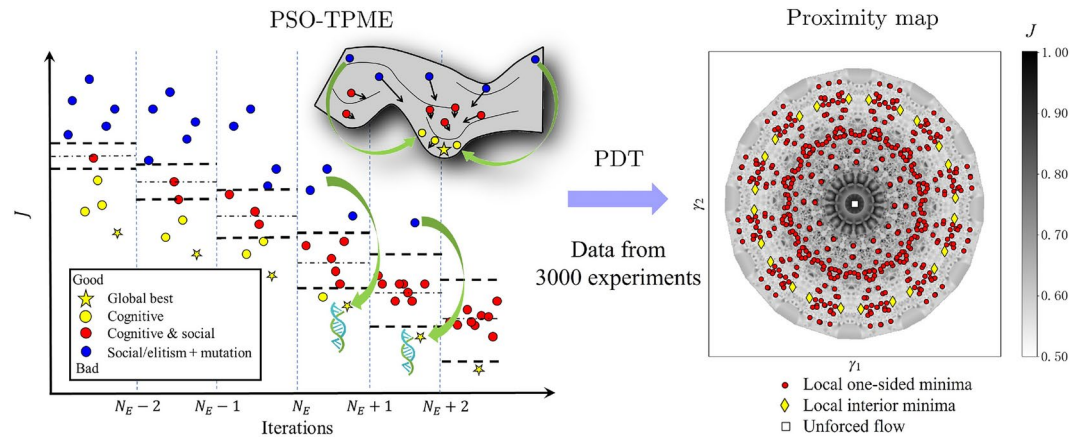
Figure 4. PSO-TPME counts on a fitness-based dynamic classifier with automated termination, elitism, and mutation. The mean particle fitness classifies particles into three categories. "Good" particles employ the cognitive model for enhanced local exploitation, "fair" particles use both cognitive and social models to balance exploration and exploitation, and "bad" particles exploit the social model to improve global exploration. Persistent "bad" particles are relocated to the position of the highest fitness particle to speed up convergence. The elite particle's position is randomly mutated to avoid local optima, enhancing diversity and fostering efficient exploration Schematic of the particle classifier and update models for each category of the PSO-TPME (left), proximity map of the augmented jet mixing data, i.e, including the points resulting from the symmetries of the problem, and minima extracted with PDT (right).
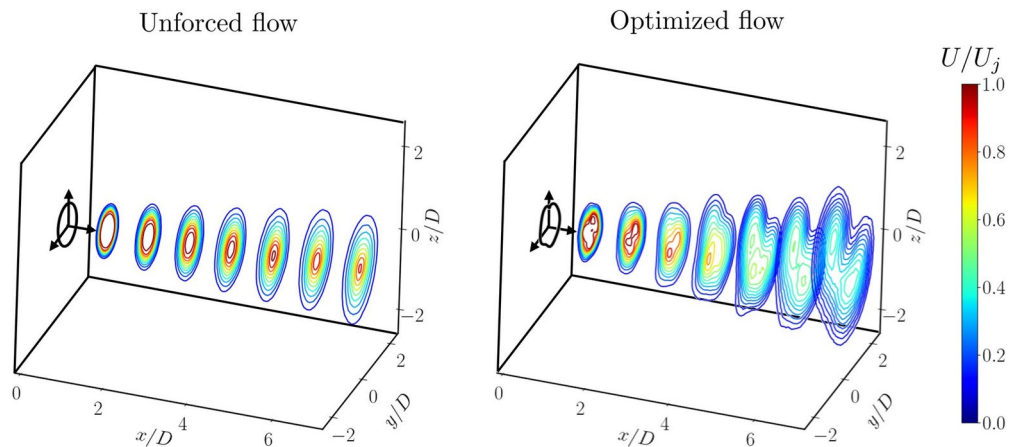

Figure 5. A comparison of normalized streamwise velocity (U/U_j) profile measured by PIV between unforced (left) and optimized (right) flows. Cross-stream contour lines represent velocity profiles at 7 cross-stream planes $x/D = 1$ to 7.

of actuators from a few to a dozen, which significantly improves the control authority over the flow. The mixing performance is characterized by the decay of the time-averaged streamwise velocity. The sensors are located near the end of the potential core following[27,28]. This gives a relatively high observability of the flow. Sensors are used to monitor the maximum velocity $U_{max} = \max_{(y,z)} (U(x = 6D, y, z))$. The cost function $J = U_{max}/U_j$ normalizes U_{max} with the jet exit velocity U_j. We also compute the jet mixing area defined by the area where $U(y, z) > 0.5\, U_{max}$ based on the PIV measurement results of the controlled flow. This particular criterion aids in quantifying the extent of effective mixing.

Given the current problem with the previously mentioned challenges, we implement the recent particle swarm optimization through targeted, position-mutated elitism (PSO-TPME)[17] on the high-dimensional jet mixing experiment. This PSO variant enhanced the convergence speed, accuracy, and global exploration capabilities of the standard PSO by at least two orders of magnitudes. PSO-TPME, depicted in Fig. 4 and detailed in the "Methods" section, can efficiently tune the particle classifier, elitism, mutation level, and mutation probability. The algorithm is appealing for the optimization of high-dimensional control parameters due to its fast convergence feature and early exploration capabilities. In addition, we compare PSO-TPME with the covariance matrix adaptation evolution strategy (CMA-ES) and Bayesian optimization (BO). PSO-TPME demonstrates
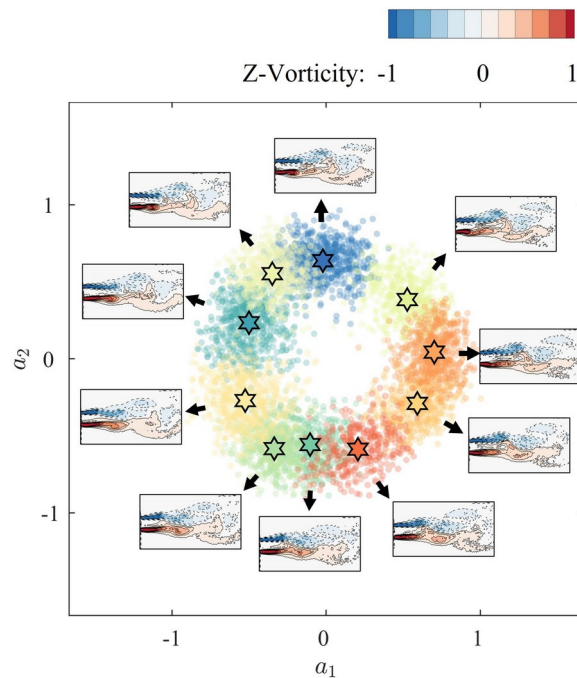
Figure 6. Cluster-based analysis of the actuated flow measured on the $z/D = 0$ plane. The snapshots and cluster centroids are projected into a two-dimensional proximity map using CMDS. The colored dots on the map represent the cluster affiliation of the snapshots, and the stars with the same color represent the corresponding cluster centroids. The centroids are visualized by the vorticity fields.
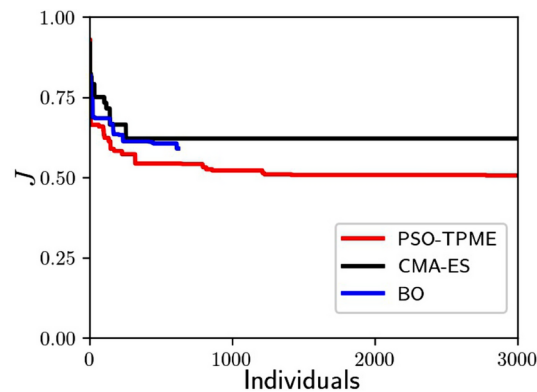
Figure 7. The learning curve of combination control (shape + active) optimizations using Smart Nozzle with different algorithms, includes PSO-TPME, CMA-ES and BO.

faster learning speed, shorter optimization times, and greater cost function reductions, the relevant results are presented in the "Methods" Section.

Finally, we analyze the topology of the 36-dimensional optimization data from PSO-TPME with persistent data topology (PDT) [26]. PDT is employed to visualize the jet-mixing dataset and extract its local, global, interior, and one-sided minima. PDT consists of two steps, the first one is extrema extraction from the dataset and the second one is smoothing the data manifold based on an elastic response model (ERM) inspired from elastic maps and nets [29]. Extrema extraction is based on a neighborhood analysis of each data point and a topological data analysis. See the "Methods" Section for more details on the methodology. At last, a proximity map based on classical multidimensional scaling (CMDS) [30] is built for a two-dimensional visualization of the high-dimensional data.

Jet mixing optimization

For jet mixing optimization, we conduct two experimental campaigns to explore the efficiency of optimizing shape variation and the combined use of both methods, respectively. In each campaign, we employ PSO-TPME to enable fast optimization in the high-dimensional parameter space. To ensure a comprehensive comparison,

we utilize the same training parameters for experimental campaigns, including 150 iterations and a particle size equivalent to 55% of the number of optimization parameters. Following the iterative training period, passive-only optimization results in a 19% reduction in the cost function. The optimized shape, as depicted in the "Shape optimization" column of Fig 3, exhibits two sharp angles on the lower left side and the higher right of the nozzle. These sharp angles will generate counter-rotating vortices in the jet flow and enhance the mixing efficiency as detailed in Quinn[1].

As a key innovation, we simultaneously optimize shape and control parameters to leverage the benefits of combining shape variation and active control. Although this configuration results in a 36-dimensional design space, PSO-TMPE efficiently tackles such high dimensionality and reduces the cost function by 47%. Compared with the active control in previous studies [7] where the centerline velocity decreased by about 30%, the optimized solution combining passive and active control can achieve a centerline velocity reduction of about 50%, significantly improving the mixing efficiency of the jet. Instead of a circular nozzle shape, the optimized shape parameters result in a wrinkled contour, and the nozzle shape is slightly squeezed at the top and lower left and slightly expanded in the bottom-right direction. For optimized active control, the azimuthal layout of optimized control parameters is the same as the optimized shape parameters. Each sector represents a minijet actuator, with the sector size indicating the duty cycle and the color representing the phase. The Strouhal number is defined by the jet nozzle diameter and outlet velocity ($St = fD/U_j$). The optimized parameters lead to a flapping-like actuation in the diagonal direction at $St = 0.10$. We also need to note that some of minijets are in closed states, that implies more sparse distributed actuation may be more effective in increasing mixing. After calculating the equivalent duty cycle, the mass flow rate of the minijet is only about 1% of that of the main jet. Re-evaluations of the optimized control parameters give similar cost reduction with at most 2% discrepancy. Finally, note that different realizations of the 36-dimensional optimization yields similar cost reduction performances with a variation of $\pm 2\%$.

The combined shape and control optimization from PSO-TPME resulted in the most significant mixing enhancement among these two experimental campaigns. Therefore, we employ PDT to examine the 36-dimensional parameter space and extract local, global, interior and one-sided minima of the optimization data. The results are displayed in Fig. 4. First, the dataset is augmented exploiting the rotation and mirror symmetries of the configuration. As a result, the global interior minimum is presented 24 times and are all identified as local interior minima by PDT. PDT also reveals 552 local one-sided minima (red dots), i.e. points whose minimality has not been established in all directions. Next, we smooth out all the spurious minima except for the global by introducing a small perturbation (anti-noise) in the data. The anti-noise level is computed with an elastic response model (ERM) so that the number of extrema is minimized. Finally, the control landscape is gradually smoothed until all the minima are flattened for a topological anti-noise level of $\varepsilon = 20.66\%$ of the cost range. The most persistent minimum, i.e. the last to be smoothed out, is the global minimum, showing that this solution is a robust feature of the control landscape.

To visualize the flow field under optimized parameters and uncover the underlying flow physics, we employ particle image velocimetry (PIV) to measure the flow fields at seven different cross-stream planes ($x/D = 1$ to 7). Fig 5 illustrates a comparison between the unforced and optimized flow fields. The unforced flow demonstrates a slow expansion of the axisymmetric shear layer, which contributes to the mixing process. However, the optimized flow exhibits more complex mixing dynamics. In contrast to the concentric circles observed in the unforced flow, the velocity contour lines (red contour lines) near the centerline on the cross-stream planes at $1D$ and $2D$ exhibit a highly tortuous shape. This deformation results from the combined effects of optimized shape design and active control parameters. The optimized shape introduces azimuthal curvature variations, producing initial streamwise vortices near the jet exit. This phenomenon is analogous to traditional non-circular jets, such as those with triangular, rectangular, square, and elliptical shapes[1,2,31,32]. In these conventional configurations, the corners cause the nozzle exit vortex ring to roll up, generating streamwise vortex pairs. In the optimized active control parameters, minijet actuators positioned at the same azimuthal angles as the wrinkles exhibit relatively high duty cycles. This suggests that minijet actuation with higher duty cycles can enhance the flow vortices induced by the wrinkled corners. Additionally, the minijets themselves can influence the nozzle exit vortex ring, causing it to roll up prematurely[7].

Despite similar duty cycles among mini jet actuators in other orientations, phase differences between them result in time delays in rolling up the outlet vortex ring, further distorting it and creating streamwise vortices. The vortices generated by the combination of active and passive control manifest as multiple wrinkles in the velocity contour line. These vortices incorporate a significant amount of ambient air and greatly improve mixing efficiency, which results in a rapid decrease in jet core velocity. Additionally, the asymmetric control rate causes the contour lines to display an asymmetric velocity field.

The distinct high-velocity contour line circle near the centerline gradually disappears, replaced by smaller velocity contour line circles. The flow asymmetry becomes more pronounced, and the jet column gradually exhibits a bifurcation phenomenon. Compared with the unforced flow, this bifurcation increases the interaction area between the jet and ambient air, strengthens the momentum exchange, and increases the mixing efficiency. Benefiting from the combination of active and passive optimization control, the optimized flow configuration yields a mixing area of 4.5 times the unforced case.

The PIV sampling frequency is far below the actuation frequency. Hence, the obtained flow field snapshots are not time-resolved. This makes DMD and POD non-viable options for the dynamics analysis. However, the employed cluster-based analysis provides an impression of the temporal sequence via the centroids. Clustering has successfully described the dynamics of numerous configurations[33,34]; it can provide quasi-temporal resolution from non-time-resolved PIV snapshots. Clustering partitions the snapshots into geometrically close subsets. The centroid of each subset serves as a representative state of the flow. Here, the k-means++ clustering algorithm is employed to coarse-grain 5000 velocity snapshots measured at the $z/D = 0$ plane into 10 clusters.

Fig. 6 shows the proximity map spanned by all the snapshots. A strongly periodic dynamics can be identified from the proximity map. The snapshots (colored dots in the figure) are distributed as a circular limit cycle, where the width of the oscillator is stable throughout the cyclic pattern, indicating a stable periodic behavior. Clustering automatically discretizes this limit cycle into 10 centroids. We infer an oscillatory behavior with a vortex-shedding from the clockwise succession of the centroids. This observation indicates that the bifurcated jet plume in Fig. 5 generates a vortex shedding that significantly enhances the jet mixing area.

Conclusions

The goal of the proposed Smart Nozzle and learning approach is to emphasize the effectiveness of biologically inspired hardware and algorithms on flow control, more precisely, jet mixing enhancement. Inspired by biology, we propose a novel jet mixing control paradigm of flexible nozzle and distributed actuators—termed the 'Smart Nozzle.' The Smart Nozzle presents a benchmark that combines passive (shape) flow control and active flow control, enabling a wide range of flow control strategies. Apart from the high potential for jet mixing enhancement, the Smart Nozzle leads to a high-dimensional control design space. PSO-TPME, a swarm intelligence algorithm, is enriched with naturally inspired operators: classification, targeted mutation, and elitism. PSO-TPME's fast-converging characteristics and early exploration capabilities make it a preferred choice for high-dimensional online optimization.

We performed two experimental 150-iteration campaigns using PSO-TPME: shape and shape + control optimization, resulting in a 19% and 47% decrease in the cost function, respectively. Compared to previous passive [7] or active flow control methods [8], which results in several percent (passive-only) or around 30% (active-only) decay of the jet centerline velocity, the combined passive and active control achieves a velocity decay of approximately 50%. This indicates that combined control strategies have significant potential in the field of jet mixing. The 36-dimensional combined shape and control optimization provide the 4.5 fold mixing area with the optimized forcing parameters (horizontally flapping mini-jets at a frequency of $St = 0.10$) and the optimal nozzle shape (slightly squeezed at the top and lower left and slightly expanded in the inclined direction). We employ persistent data topology (PDT) to analyze the 36-dimensional combined shape and control optimization dataset and extract 552 local one-sided minima. PDT is a new neighborhood and topological data analysis-based approach[26]. The topological features extracted by PDT suggest the most fitting optimization algorithm and guide the development of a surrogate model. We believe that future optimization algorithms will get insight from the data topology. PDT concluded the robustness of the optimization because one global minimum (detected by PSO-TPME) remained after smoothing the control landscape with a topological anti-noise level of $\varepsilon = 20.66\%$ of the cost range. Using 5000 streamwise PIV images of the actuated flow, we employed the unsupervised k-means++ algorithm with 10 clusters to coarse-grain the snapshots. The cluster-based analysis recognized the strongly periodic dynamics of the dominant flow field (the dancing jet). The current study demonstrates unprecedented jet-mixing performances thanks to a high-dimensional experimental opportunity space comprising shape optimization, passive and active control combined with the powerful algorithms of artificial intelligence.

Despite the significant mixing effect achieved by the current optimization results, it is important to highlight the challenges associated with optimization algorithms. There is no guarantee to converge at the global optimimum given the topologically complex search space. Similarly, the algorithm is sensitive to meta parameters. We mitigated these risks with numerous repeated optimization experiments. In all cases, PSO-TPME features a similar learning rate and cost function descent, suggesting convergence at or near the global optimal. Other employed algorithms, like Bayesian optimization and CMA-ES, exhibited a distinctly slower descent. Further research will explore the Reynolds number effect on this bio-inspired hybrid (passive + active) jet mixing optimization. One goal is the optimization performance of a given algorithm across various Reynolds numbers and examine the potential scaling relationship between active and passive control parameters (such as number of corners, active control frequency, etc.) and Reynolds number.

Biologically inspired active and passive control of jet mixing can be expected to help in prototyping simpler and similarly effective mixing applications. Examples are dilution jets in aeroengines and fuel nozzles to enhance combustion efficiency [4]. Other examples include mixing of pollutants with the surrounding air to reduce concentration and minimize the harm caused by pollutants. Furthermore, the simultaneous optimization of active and passive control as myriad of other applications, e.g. separation delay over wings and in diffusers.

Methods

Particle swarm optimization through targeted, position-mutated, elitism (PSO-TPME)

Kennedy and Eberhart[35] pioneered metaheuristic particle swarm optimization (PSO). The PSO technique emulates the dynamics of biological systems like a flock of birds. The PSO's low memory requirements and ease of use motivate the PSO implementation in several multidimensional, complex applications that incorporate optimization, artificial intelligence, data-driven control, etc.

Initially, the particle swarm optimization method generates a swarm of particles at uniformly random locations to explore the search space. Hence, PSO updates the particle locations over the course of iterations (It) to enhance the global fitness value of an optimization problem. The update of the particles' positions (x_{ij}) and velocities (v_{ij}) relies on the particle's cognitive component, which is the particle's thus far best fitness value, referred to as "personal best" (P_b). Furthermore, the update depends on the swarm's social component, which is the swarm's best fitness value, known as the "global best" (G_b). One basic version of PSO reads:

$$v_{ij}^{k+1} = wv_{ij}^k + c_1r_1(P_{bij} - x_{ij}^k) + c_2r_2(G_{bj} - x_{ij}^k) \tag{1}$$

$$x_{ij}^{k+1} = x_{ij}^k + v_{ij}^{k+1} \tag{2}$$

$$w = w_{\max} - It \times \frac{(w_{\max} - w_{\min})}{It_{\max}} \tag{3}$$

where $i \in [1, N]$ indicates the particle index and $j \in [1, n]$ its j-th component. N and n being the total number of particles and n the dimension of the problem, respectively.

The inertia weight is defined by w, and the maximum and minimum inertia weights are denoted by $w_{\max}$ and $w_{\min}$, respectively. The cognitive and social acceleration factors are c_1 and c_2, respectively, whereas r_1 and r_2 are randomly generated values from 0 to 1.

PSO is effective in optimizing complex systems[36], but it has a sluggish convergence rate[37–41] as well as premature convergence and stagnation to local optima[37–39,41–43].

Shaqarin and Noack[17], introduce a new PSO variant (PSO-TPME) that enhanced the convergence speed and global exploration capabilities of the conventional PSO by at least two orders of magnitudes. They report significant enhancement of the convergence speed, accuracy, and early exploration capabilities within the first 10 iterations. PSO-TPME demonstrated its real-time optimization-based control capabilities for partially shaded photovoltaic (PV) systems[44]. PSO-TPME approach is shown in algorithm 1, which has three main features described below.

Classification
PSO-TPME relies on fitness-based adaptive classification with convergence-based automatic termination. Over the course of iterations, the algorithm calculates the swarm's average fitness value (m). Then, it generates lower and upper limits based on a predetermined proportion (p) around the mean that classifies the particles into three classes: good, fair, and bad if their fitness (f) is less than the lower limit, in between the limits, or higher than the upper limit, respectively. The algorithm reduces the velocities of the "good" particles using the cognitive model to boost their exploitation capabilities, whereas PSO-TPME uses the social model to elevate the "bad" particles' velocities to improve their exploration capabilities. The complete model continues to update the "fair" particles to balance their exploration and exploitation abilities.

Elitism
Elitism is the operation of substitution of "bad" particles by particles with the best fitness values after a defined number of iterations, culminating in the formation of a new swarm with better average fitness. This procedure will undoubtedly accelerate convergence, but it will reduce particle diversity and raise the likelihood of stagnation into a local optimum.

In PSO-TPME, "bad" particles remained classified as "bad" and failed to advance to a higher class after a certain number of iterations (N_e) with full exploration capabilities, referred to as "hopeless particles." The algorithm initiates the elitism process to deal with "hopeless particles" and speed up convergence. The "hopeless particles" are now assigned to the particle's location with the best fitness ($f_{\max}$).

Mutation
The mutation is a biologically inspired operator that improves convergence speed and accuracy by improving particle diversity. Inclusion of a mutation to the particle's location of the best fitness ($x_j(f_{\max})$) soon after elitism will improve the diversity of the elite particle, limit the likelihood of slipping into a local optimum, and enhance convergence accuracy. Correspondingly, mutation now exclusively targets "bad" particles with mutation probability (mp), and mutation occurs directly on the particle's location rather than indirectly.

Swarm Initialization
Initialize personal best (P_{bij}) **and global best** (G_{bj})
for $It = 1$ to $It_{\max}$ **do**
    for $i = 1$ to N_{pop} **do**
        if $f_{ij}^k < (1-p)m$ **then**
            $v_{ij}^{k+1} = wv_{ij}^k + c_1 r_1 (P_{bij} - x_{ij}^k)$
            $x_{ij}^{k+1} = x_{ij}^k + v_{ij}^{k+1}$
        else if $(1-p)m \le f_{ij}^k \le (1+p)m$ **then**
            $v_{ij}^{k+1} = wv_{ij}^k + c_1 r_1 (P_{bij} - x_{ij}^k) + c_2 r_2 (G_{bj} - x_{ij}^k)$
            $x_{ij}^{k+1} = x_{ij}^k + v_{ij}^{k+1}$
        else if $f_{ij}^k > (1+p)m$ **then**
            $v_{ij}^{k+1} = wv_{ij}^k + c_2 r_2 (G_{bj} - x_{ij}^k)$
            $x_{ij}^{k+1} = x_{ij}^k + v_{ij}^{k+1}$
        else if $f_{ij}^k > (1+p)m$ & $It \ge N_e$ & $\eta < mp$ **then**
            $x_{ij}^{k+1} = x_j(f_{\max})(2a\eta + (1-a))$
        end if
        if $f(P_{bij}) < f(x_{ij})$ **then**
            $P_{bij} \leftarrow f(x_{ij})$
            if $f(G_{bj}) < f(P_{bij})$ **then**
                $G_{bj} \leftarrow f(P_{bij})$
            end if
        end if
    end for
    $w \leftarrow w_{\max} - It \times \frac{(w_{\max} - w_{\min})}{It_{\max}}$
end for

Algorithm 1. PSO-TPME (Minimization) See Fig. 3.

Persistent data topology (PDT)

PDT is inspired by discrete scalar-field topology and enables topological feature identification in high dimensions. PDT consists of two steps: First, the extrema of the data are identified based on a neighborhood analysis. Second, the persistency of the extrema, or the 'depth'/'height' of the minima/maxima, is evaluated with an elastic response model (ERM) inspired by elastic maps and nets [29]. A point $\mathbf{x}_i \in \mathscr{R}^n$ with cost J_i is a local interior minimum if (1) at least the $n+1$ nearest neighbors have a higher cost value than J_i and (2) the nearest neighbors define a convex hull that includes $\mathbf{x}_i$. When the second condition is not satisfied, $\mathbf{x}_i$ is called a local one-sided minimum. The global interior minimum is then a local interior minimum whose cost is the smallest of the whole data set. The global one-sided minimum has the smallest cost but the second condition is not fulfilled. Local, global, interior, and one-sided maxima are defined analogously. These definitions are higher-dimensional generalizations of the conventional one-dimensional definitions inspired by discrete scalar-field topology [45]. The ERM minimizes the number of extrema with a topological anti-noise introduced on the cost J. 'Spurious' extrema of the data are likely to be smoothed out by low levels of topological anti-noise, while deep or high extrema tends to persist for high levels of topological anti-noise. Details are provided in Ref. [26,46].

Experimental setup

To achieve combined shape variation and active control for jet mixing enhancement, we design the Smart Nozzle, as illustrated in Fig 2. The Smart Nozzle comprises two primary components: a contoured nozzle and a flexible nozzle. The contoured nozzle is 80 mm long and the exit diameter is 50 mm. The inner profile is a third-order polynomial with a contraction ratio of 1:4. The flexible nozzle, which is a 65mm long straight nozzle made of soft material (silica gel), is installed in front of the contoured nozzle. The flexibility of the Smart Nozzle is crucial for achieving various passive control capabilities, allowing for the customization of the nozzle exit shape. Shape variation and active control are both achieved by this add-on flexible nozzle.

To control nozzle shape deformation, we utilize 12 stepper motors to stretch or squeeze the flexible nozzle for shape variation. These stepper motors are equidistantly mounted on a concentric shroud. For active flow control, we deploy 12 minijets actuators at the periphery of the flexible nozzle exit. Each minijet is regulated by a solenoid valve, and the air source of the minijets comes from a constant-pressure compressed air tank. We install the Smart Nozzle on a chamber with steel-wire meshes and a honeycomb flow straightener to create uniform flow at the nozzle exit. The jet facility is placed in an air-conditioned laboratory where the room temperature remains constant within $25 \pm 1\,^\circ$C. Both the jet flow and environment air are regular air with a density of $\rho \approx 1.18\,\mathrm{kg m^{-3}}$. The air supply comes from a 2.2 kW axial fan. A PID controller is implemented to regulate the jet exit velocity at $U_j = 8\,\mathrm{m/s}$, which corresponds to a Reynolds number of $Re_D \approx 2.5 \times 10^4$ for the unforced flow. This specific

value was selected to ensure a turbulent flow regime, which is more representative of the conditions typically encountered in industrial applications. Moreover, our choice is guided by previous[2,31] literature that frequently employs similar Reynolds numbers for comparable experiments.

To evaluate the mixing efficiency, we position an array of 7×7 velocity probes at 6 jet diameters downstream. The probes are connected to a 64-channel pressure scanner (Hanghua PSU-64). We calculate the maximum mean streamwise velocity based on the pressure readings and employ an estimate of the velocity decay as the cost function $J = \max_{(y,z)}(U(x = 6D, y, z))/U_j$.

The jet mixing enhancement experiments require independent control of each stepper motor and each solenoid valve. We utilize a National Instruments (NI) PCIe 6325 card, such that the motion of each stepper motor, as well as the frequency, duty cycle, and phase of each minijet can be individually commanded. In this work, we enable independent control of all 12 stepper motors and periodically excite the flow using a uniform frequency with 12 duty cycles and 11 phase differences. This results in a flow control optimization problem with a total of 36 parameters.

To obtain a spatially resolved velocity field, we conduct PIV measurements. Streamwise velocity fields are measured using planar PIV, while velocity fields on cross-stream planes are acquired using stereoscopic PIV. For planar PIV, the camera is positioned perpendicular to the plane of the light sheet. In contrast, for stereoscopic cross-stream measurements, two cameras are oriented at approximately $43°$ to the light sheet. Scheimpflug adapters are used to ensure that the full field of view is in focus. Both ambient air and jet flow are seeded with Di-Ethyl-Hexyl-Sebacate (DEHS, density $\rho \approx 0.91\,\mathrm{g/cm^3}$, $d \approx 0.2\,\mathrm{\mu m}$). A dual-cavity Litron Nd:YAG laser serves as the light source, operating at a wavelength of 532 nm. Two LaVision CCD cameras (Imager SX 6M, 2752 pixels $\times$ 2200 pixels) are used to capture images. All post-processing is performed using LaVision DaVis 10.2 software. Image pairs are sampled at 12 Hz, and the velocity fields are calculated through multiple passes with decreasing interrogation window sizes. The interrogation window size for the final pass is 32 pixels $\times$ 32 pixels with 75% overlap. The average uncertainty in the measurement of the velocity field is less than 2%.

Additionally, we employ various optimization algorithms to perform the combined active-passive optimization of the smart nozzle, the relevant learning curve is shown in Fig 7. Given that each algorithm has different iteration parameters, we use the number of individuals as the x-axis, with each individual representing a new control rate attempt. The three algorithms-PSO-TPME, CMA-ES, and BO-are executed on the same computer, with all hardware being identical except for the algorithm itself. During the optimization process, BO takes an increasing amount of time to determine the next query point to evaluate. After 600 evaluations, this time has reached 20 minutes per individual making further optimization impractical. In contrast, both the PSO-TPME and CMA-ES algorithms require only tens of seconds per individual. Furthermore, PSO-TPME demonstrated a faster optimization rate and greater efficiency.

Data availability
The datasets used and/or analysed during the current study available from the corresponding author on reasonable request.

References
1. Quinn, W. R. Measurements in the near flow field of an isosceles triangular turbulent free jet. *Exp. Fluids* **39**, 111–126 (2005).
2. Quinn, W. R. Turbulent mixing in a free jet issuing from a low aspect ratio contoured rectangular nozzle. *Aeronaut. J.* **99**, 337–342. https://doi.org/10.1017/s000192400002858x (1995).
3. Rathakrishnan, E. Effect of tab length on supersonic jet mixing. *Phys. Fluids* https://doi.org/10.1063/5.0113192 (2022).
4. Sun, L., Bian, F., Lei, X., Shi, D. & Bao, F. Quantitative analysis of enhanced mixing and combustion by lobed mixer in a ramjet engine: Study using hyperbolic Lagrangian coherent structures. *Aerosp. Sci. Technol.* **140**, 108471. https://doi.org/10.1016/j.ast.2023.108471 (2023).
5. Gad-el Hak, I. & Mureithi, N. Mitigation of jet cross-flow induced vibrations using an innovative biomimetic nozzle design inspired by shark gill geometry. *Sci. Rep.* **12**, 11107 (2022).
6. Samimy, M., Kim, J.-H., Kastner, J, Adamovich, I. & Utkin, Y. Active control of a Mach 0.9 jet for noise mitigation using plasma actuators. *AIAA J.* **45**, 890–901. https://doi.org/10.2514/1.27499 (2007).
7. Yang, H. & Zhou, Y. Axisymmetric jet manipulated using two unsteady minijets. *J. Fluid Mech.* **808**, 362–396. https://doi.org/10.1017/jfm.2016.634 (2016).
8. Ho, C.-M. & Gutmark, E. Vortex induction and mass entrainment in a small-aspect-ratio elliptic jet. *J. Fluid Mech.* **179**, 383–405. https://doi.org/10.1017/s0022112087001587 (1987).
9. Novati, G., de Laroussilhe, H. L. & Koumoutsakos, P. Automating turbulence modelling by multi-agent reinforcement learning. *Nat. Mach. Intell.* **3**, 87–96 (2021).
10. Fan, D., Yang, L., Wang, Z., Triantafyllou, M. S. & Karniadakis, G. E. Reinforcement learning for bluff body active flow control in experiments and simulations. *Proc. Natl. Acad. Sci.* **117**, 26091–26098 (2020).
11. Fan, D., Zhang, B., Zhou, Y. & Noack, B. R. Optimization and sensitivity analysis of active drag reduction of a square-back Ahmed body using machine learning control. *Phys. Fluids* **32**, 125117 (2020).
12. Garnier, P. et al. A review on deep reinforcement learning for fluid mechanics. *Comput. Fluids* **225**, 104973 (2021).
13. Vinuesa, R., Lehmkuhl, O., Lozano-Durán, A. & Rabault, J. Flow control in wings and discovery of novel approaches via deep reinforcement learning. *Fluids* **7**, 62 (2022).
14. Wu, M.-Y. et al. Airfoil shape optimization using genetic algorithm coupled deep neural networks. *Phys. Fluids* https://doi.org/10.1063/5.0160954 (2023).
15. Koumoutsakos, P., Freund, J. & Parekh, D. Evolution strategies for automatic optimization of jet mixing. *AIAA J.* **39**, 967–969 (2001).
16. Xu, F. et al. The optimization for the backward-facing step flow control with synthetic jet based on experiment. *Exp. Thermal Fluid Sci.* **64**, 94–107 (2015).

17. Shaqarin, T. & Noack, B. R. A fast-converging particle swarm optimization through targeted, position-mutated, elitism (PSO-TPME). *Int. J. Comput. Intell. Syst.* **16**, 6 (2023).
18. Wang, D., Tan, D. & Liu, L. Particle swarm optimization algorithm: An overview. *Soft. Comput.* **22**, 387–408. https://doi.org/10.1007/s00500-016-2474-6 (2017).
19. Jordan, P. & Colonius, T. Wave packets and turbulent jet noise. *Annu. Rev. Fluid Mech.* **45**, 173–195 (2013).
20. Cavalieri, A. V., Jordan, P. & Lesshafft, L. Wave-packet models for jet dynamics and sound radiation. *Appl. Mech. Rev.* **71**, 020802 (2019).
21. Li, Z. et al. The effect of sinusoidal wall on hydrogen jet mixing rate considering supersonic flow. *Energy* **193**, 116801 (2020).
22. Peng, Y. et al. Mixing enhancement of the multi hydrogen fuel jets by the backward step. *Energy* **203**, 117859 (2020).
23. Power, G., McClure, M. & Vinh, D. Advanced IR suppresser design using a combined CFD test approach. AIAA paper 94–3215 (1994).
24. Smith, L. et al. Mixing enhancement in a lobed injector. *Phys. Fluids* **9**, 667–678 (1997).
25. Ranadive, P., Parulkar, A. & Brunelli, N. A. Jet-mixing reactor for the production of monodisperse silver nanoparticles using a reduced amount of capping agent. *React. Chem. Eng.* **4**, 1779–1789 (2019).
26. Wang, T., Cornejo Maceda, G. Y. & Noack, B. R. *xPDT: a Toolkit for Persistent Data Topology, vol. 3 of Machine Learning Tools in Fluid Mechanics* 1st edn. (Technische Universität Braunschweig, Braunschweig, 2023).
27. Zhou, Y., Fan, D., Zhang, B., Li, R. & Noack, B. R. Artificial intelligence control of a turbulent jet. *J. Fluid Mech.* https://doi.org/10.1017/jfm.2020.392 (2020).
28. Fan, D. W., Wu, Z., Yang, H., Li, J. D. & Zhou, Y. Modified extremum-seeking closed-loop system for jet mixing enhancement. *AIAA J.* **55**, 3891–3902. https://doi.org/10.2514/1.j055644 (2017).
29. Gorban, A. N. & Zinovyev, A. Y. Elastic maps and nets for approximating principal manifolds and their application to microarray data visualization. arXiv: arXiv:0801.0168v1. Data Analysis, Statistics and Probability (2007).
30. Wickelmaier, F. *An introduction to MDS.* No. R00-6003 in Aalborg Universitetscenter. Institut for Elektroniske Systemer. Afdeling for Kommunikationsteknologi. Rapport (Aalborg Universitetsforlag, 2003).
31. Quinn, W. R. Streamwise evolution of a square jet cross section. *AIAA J.* **30**, 2852–2857. https://doi.org/10.2514/3.48973 (1992).
32. Husain, H. S. & Hussain, F. Elliptic jets. Part 2. Dynamics of coherent structures: Pairing. *J. Fluid Mech.* **233**, 439–482. https://doi.org/10.1017/s0022112091000551 (1991).
33. Kaiser, E. et al. Cluster-based reduced-order modelling of a mixing layer. *J. Fluid Mech.* **754**, 365–414 (2014).
34. Fernex, D., Noack, B. R. & Semaan, R. Cluster-based network modeling-from snapshots to complex dynamical systems. *Sci. Adv.* **7**, eabf5006 (2021).
35. Kennedy, J. & Eberhart, R. Particle swarm optimization. In *Proceedings of ICNN'95-international conference on neural networks*, vol. 4 1942–1948 (IEEE, 1995).
36. Huang, K.-W. et al. Memetic particle gravitation optimization algorithm for solving clustering problems. *IEEE Access* **7**, 80950–80968 (2019).
37. Jiao, W., Liu, G. & Liu, D. Elite particle swarm optimization with mutation. In *2008 Asia Simulation Conference-7th International Conference on System Simulation and Scientific Computing* 800–803 (IEEE, 2008).
38. Chen, G. *Simplified particle swarm optimization algorithm based on particles classification*, vol. 5 2701–2705 (IEEE, 2010).
39. He, Y., Chen, W., Lei, K., Zhao, Y. & Lv, P. Semi-airborne electromagnetic 2.5 D inversion based on a PSO-LCI strategy. *J. Appl. Geophys.* **197**, 104541 (2022).
40. Liu, S., Liang, M. & Hu, X. Particle swarm optimization inversion of magnetic data: Field examples from iron ore deposits in China. *Geophysics* **83**, J43–J59 (2018).
41. Ramírez-Ochoa, D.-D., Pérez-Domínguez, L. A., Martínez-Gómez, E.-A. & Luviano-Cruz, D. PSO, a swarm intelligence-based evolutionary algorithm as a decision-making strategy: A review. *Symmetry* **14**, 455 (2022).
42. Liu, Q., Wei, W., Yuan, H., Zhan, Z.-H. & Li, Y. Topology selection for particle swarm optimization. *Inf. Sci.* **363**, 154–173 (2016).
43. Pahnehkolaei, S. M. A., Alfi, A. & Machado, J. T. Analytical stability analysis of the fractional-order particle swarm optimization algorithm. *Chaos Solitons Fractals* **155**, 111658 (2022).
44. Shaqarin, T. Particle swarm optimization with targeted position-mutated elitism (PSO-TPME) for partially shaded PV systems. *Sustainability* **15**, 3993 (2023).
45. Kasten, J. et al. Acceleration feature points of unsteady shear flows. *Arch. Mech.* **68**, 55–80 (2016).
46. Wang, T. et al. Topologically assisted optimization for rotor design. *Phys. Fluids* **35**, 055105. https://doi.org/10.1063/5.0145941 (2023).

Acknowledgements

Author contributions

B.R.N., N.G., T.S. and Z.T. conceived the experiment(s), Z.T., N.G. and G.Y. conducted the experiment(s), T.Y., C.H. and N.D. analysed the results. All authors reviewed the manuscript.

Declarations

Competing interests

The authors declare no competing interests.

Additional information

Correspondence and requests for materials should be addressed to G.Y.C.M. or B.R.N.

Reprints and permissions information is available at www.nature.com/reprints.

Publisher's note Springer Nature remains neutral with regard to jurisdictional claims in published maps and institutional affiliations.